Assessing Curl-Conforming Bases for Pyramid Cells

Assessing Curl-Conforming Bases for Pyramid Cells

Roberto D. Graglia, *Life Fellow, IEEE*, and Paolo Petrini, *Member, IEEE*

***Abstract*—Successful three-dimensional finite element codes for Maxwell's equations must include and deal with all four types of geometrical shapes: tetrahedra, bricks, prisms, and quadrangular-based pyramids. However, pyramidal elements have so far been used very rarely because the basis functions associated with them have complicated expression, are complex in derivation, and have never been comprehensively validated. We recently published a simpler procedure for constructing higher-order vector bases for pyramid elements, so here we fill a gap by discussing a whole set of test case results that not only validate our new curl-conforming bases for pyramids, but which enable validation of other codes that use pyramidal elements for finite element method applications. The solutions of the various test cases are obtained using either higher order elements or multipyramidal meshes or both. Furthermore, the results are always compared with the solutions obtained with classical tetrahedral meshes using higher order bases. This allows us to verify that purely pyramidal meshes and elements give numerical results of comparable accuracy to those obtained with multitetrahedral meshes that use elements of the same order, essentially requiring the same number of degrees of freedom. The various results provided here also show that higher order vector bases always guarantee a superior convergence of the numerical results as the number of degrees of freedom increases.**

***Index Terms*—Electromagnetic fields, finite-element methods, higher order vector elements, pyramidal elements, numerical analysis.**

I. Introduction

ALMOST all practitioners of computational electromagnetics (CEM) avoid using pyramidal cells because the related vector bases are very complicated and never extensively tested; in fact very few authors have used pyramids so far, as can be seen from [1], [2], [3] and references therein. This has hindered the development of codes that use hybrid meshes smoothly; that is, meshes that employ higher-order pyramidal elements in addition to tetrahedra, bricks, and prisms, despite the fact that a reasonably extensive scientific literature on higher-order pyramidal elements has developed over the past twenty years [4]-[11]. Things may now change, firstly because the method in [1], [2] to obtain conforming bases of arbitrarily high order for pyramids is, in our opinion, decidedly simpler than those previously available in the literature. Secondly because this paper fills the lack of useful test cases for validating numerical codes that use pyramid cells, or at least their curl-conforming bases for Finite Element Method (FEM) applications.

In fact, this paper assesses the modeling capabilities of the higher order bases for pyramid cells reported in [1], which differ from those in [3], presenting several results for pyramidal and rectangular cavity resonators useful for validating computer codes that use these cells and bases. This is done because cavity problems are the best benchmark for immediately checking whether a (new) basis avoids spurious modes or not. More specifically, this paper considers rectangular electromagnetic resonators for two very good reasons: first because they have a known and very simple solution, and second because their geometry can be meshed using only pyramids. The results obtained here add to those in [1] where we modeled a few pyramidal cavities with a single cell.

The fields inside the volume V of a closed metal cavity and the corresponding wavenumbers k are modeled by the vector Helmholtz equation whose discretization produces a generalized matrix eigenvalue equation $\mathbf{Ae} = k^2\mathbf{Be}$ with entries [12, Sections 6.5, 6.6]

$$A_{mn} = \iiint_V \frac{1}{\mu_\mathrm{r}} \nabla \times \boldsymbol{B}_m \cdot \nabla \times \boldsymbol{B}_n \mathrm{d}V \tag{1}$$

and

$$B_{mn} = \iiint_V \varepsilon_\mathrm{r} \boldsymbol{B}_m \cdot \boldsymbol{B}_n \mathrm{d}V \tag{2}$$

$\boldsymbol{B}_m$ and $\boldsymbol{B}_n$ being vector basis functions. In the following we assume the material inside the cavity to be homogeneous with unitary relative permeability μ_r and relative permittivity ε_r.

The wavenumbers k are computed by means of a FORTRAN code that uses the LAPACK library and the routine DSPGV. In common with standard finite element implementations, the system of equations is usually constructed in a cell-by-cell manner where the integrals in (1) and (2) are evaluated throughout a single cell for all combinations of basis and testing functions, stored in a temporary "element matrix," and systematically transferred to the global system of equations.

This FEM technique can be applied to any conforming mesh made with a mixture of cells of different size and shape (that is tetrahedrons, prisms, bricks and pyramids), provided that curl-conforming bases are used, as required by (1). Obviously, we refer to implementations that use also higher order bases.

Recall that all elements have shape functions and basis functions of polynomial form in the so-called *"parent"* space [12], with the exception of pyramid elements which must have shape-functions and basis functions of fractional form for conformity with the other cells and to guarantee cell-to-cell tangential continuity, even in the case of curved cells [1]. (In the parent space, the divergence-conforming basis functions of the pyramid

Manuscript received 20 September 2023; revised 9 November 2023; accepted 13 November 2023. Date of publication 16 November 2023; date of current version 24 November 2023. This work was supported in part by PRIN under Grant 2017NT5W7Z GREEN TAGS, and in part by the European Union under the Italian National Recovery and Resilience Plan of NextGenerationEU through Program "Telecommunications of the Future" (PE00000001- program "RESTART") and the Program PNRR M4C2 "Multiscale modeling and Engineering Applications" of the National Centre for HPC, Big Data and Quantum Computing under Grant HPC-CUP E13C22000990001. *(Corresponding author: Roberto D. Graglia.)*

The authors are with the Dipartimento di Elettronica e Telecomunicazioni, Politecnico di Torino, 10129 Torino, Italy (e-mail: roberto.graglia@polito.it; paolo.petrini@polito.it).

Digital Object Identifier 10.1109/JMMCT.2023.3333563

TABLE I
FIRST SIX WAVENUMBERS OF THE EQUILATERAL PYRAMID-SHAPED CAVITY

Meshing with 1 pyramid									Meshing with 4 tetrahedrons						
$p=6$	5	4	3	2	1	0	**ME**	**WN**	$p=6$	5	4	3	2	1	0
5.78020	5.7802	5.780	5.78	5.81	6.03	6.32	**1**	**5.78024**	5.78028	5.7803	5.780	5.78	5.82	5.64	6.32
7.59660	7.5965	7.597	7.60	7.70	7.75	7.63	**2**	**7.59677**	7.59694	7.5969	7.596	7.60	7.61	7.44	7.30
9.26438	9.2650	9.283	9.32	9.93	10.10	N/A	**2**	**9.26451**	9.26464	9.2659	9.266	9.33	9.30	9.48	8.00
9.49191	9.4963	9.503	9.57	9.71	9.23	9.26	**1**	**9.49216**	9.49240	9.4903	9.502	9.39	9.67	8.53	11.31
1064	678	400	212	96	34	8		**DoF**	1015	678	425	244	123	50	13
700	444	260	136	60	20	4		**Non-zero EVs**	672	448	280	160	80	32	8
364	234	140	76	36	14	4		**Zero EVs**	343	230	145	84	43	18	5
360k	160k	64k	23k	4.4k	750	7		**CN**	840k	290k	86k	21k	3.3k	320	10

The upper part of the Table shows the first wavenumbers; i.e., the first six non-zero eigenvalues (EV) of the pyramidal cavity with edges of equal length, calculated with bases of order p from 0 to 6. The results on the left are obtained by meshing the cavity with a single pyramidal cell, those on the right by meshing the cavity with four identical tetrahedral cells. In the central columns, in bold, we report the multiplicity of eigenvalues (ME) together with the reference wavenumber (WN) which we can use to calculate the errors for the different values of p. The reference WN is simply the average of the two values obtained using the two different meshes with $p=6$. Notice that with so few cells the wavenumbers are in ascending order, with correct multiplicity, only for $p \geq 3$ and $p \geq 2$ in the left and right subtables, respectively. The lower part of the Table shows, for each order p, the number of degrees of freedom (DoF), the number of zero and non-zero EVs, and the value of the mass-matrix condition number (CN).

element have fractional form to guarantee the continuity of the normal component of the field from cell to cell [2]).

For pyramids, the shape functions and basis functions take polynomial form in a different space, called *"grandparent"* space, where all the pyramid cells are mapped by a cube of unit side [1], [2]. The polynomial order of the functions in the grandparent domain for the pyramid elements and in the parent domain for the other non-pyramidal elements is denoted by the integer p. For any polynomial order p, the curl-conforming functions are tangentially continuous on the boundaries in common to adjacent cells of different shape [1].

For greater clarity we recall that the use of pyramidal elements requires two mappings. The first from parent space to the observer's space (the so-called child space). The second from grandparent space to parent space. The Jacobian of the first mapping depends on the shape of the pyramidal cell in the child space, that of the second does not and is always given by the same polynomial term; see [1, eq. (11)]. As happens for other elements, the *unitary basis vectors* of the pyramidal cell are obtained by differentiating the element position vector $\boldsymbol{r}$ with respect to three independent parent coordinates [1]. From these vectors, as shown in [1 Table I], one gets the gradient vectors and the edge vectors that appear in the expression of the vector basis functions and their curls. Now, unlike what is usually done with the other elements, the FEM-matrix entries (1, 2) associated to pyramids are always computed by integrating polynomials in the grandparent domain [1], and not by integrating the "corresponding" fractional functions in the parent domain. However, the software used to produce the results presented in this paper is not optimized; that is, we trivially compute the volume FEM integrals by numerical integration on the unit cube of the grandparent domain along three directions, in cascade, without using sophisticated integration schemes that can reduce computation times [9], [13].

The rest of the paper is structured as follows. Section II provides several results related to a pyramid-shaped cavity resonator with unit sides, meshed with a single cell or multiple pyramidal cells of different aspect ratios. The numerical results are validated against those of a different code that uses higher-order tetrahedral elements. Section III reports several results for rectangular cavity resonators meshed by pyramidal cells and compares them with the well-known exact analytical solution. Also, in Section III, the accuracy of the results obtained using only pyramidal cells is compared with that obtained from the code using higher order tetrahedral elements. In summary, in this paper we use meshes formed only by quadrangular-based pyramidal cells; unlike what happens when pyramids are used (albeit rarely) as *"fillers"* of hybrid meshes; that is, as gluing elements inserted between other non-pyramidal cells. Readers may find it helpful to review [1], [2], for a detailed introduction to the notation and other background information. Preliminar results of this work were presented in [14].

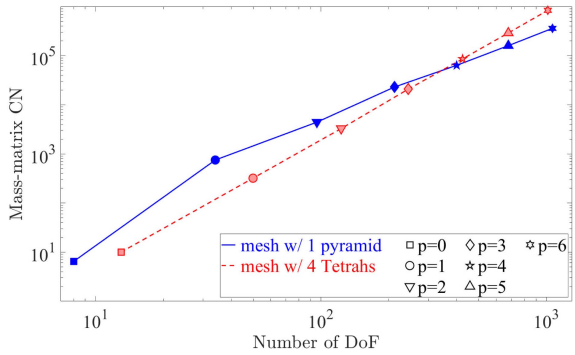

Fig. 1. Condition Number (CN) of the mass-matrix versus the number of degrees of freedom obtained using bases of order p from 0 to 6 by meshing an equilateral pyramid with a single pyramidal element (in blue), or with four identical tetrahedral elements (in red).

II. RESULTS FOR THE EQUILATERAL PYRAMID

Table I reports the first six wavenumbers of an equilateral pyramid-shaped cavity obtained with bases of order p from 0 to 6, while Fig. 1 shows the trend of the condition number of the mass-matrix as the order used varies. The results obtained by meshing the cavity with a single pyramidal cell are compared in Table I with those obtained using four identical tetrahedral

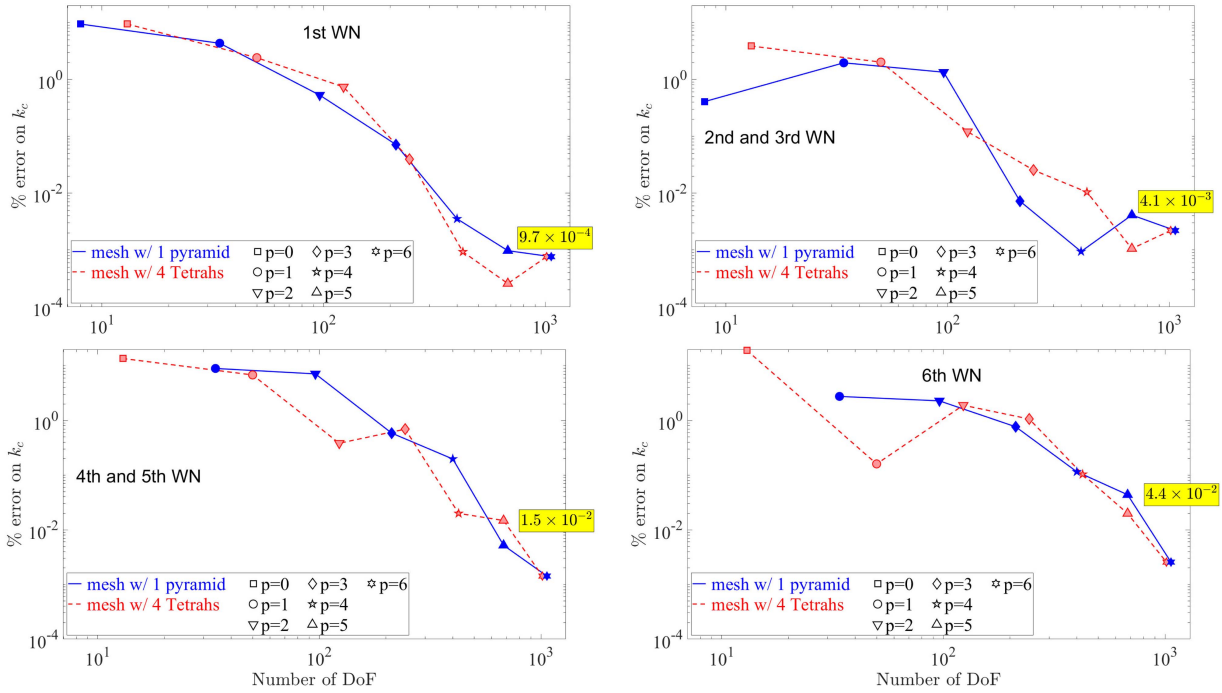

Fig. 2. Percentage errors for the first 6 wavenumbers of an equilateral pyramid versus the number of degrees of freedom. Errors refer to Table I results obtained for p between 0 and 6, and are computed against the WN result reported in bold in the middle column of Table I. The second and third modes of the cavity have identical wavenumbers, as do the fourth and fifth modes. For $p = 0$, a single pyramid cell yields only four non-zero eigenvalues; for this $p = 0$ case we show with a blue square marker the errors of the first three modes only.

cells, as done in [1 Table VII] for bases up to third order. The Table results show that

- for $p \geq 3$ we can sort the first six wavenumbers of the cavity in ascending order and with the correct multiplicity, regardless of the mesh we have used;
- for $p \geq 5$ the number of zero eigenvalues obtained with a single pyramid cell is higher than that obtained with 4 tetrahedral cells;
- for $p \geq 6$ the number of degrees of freedom (DoF) obtained by meshing the structure with a single pyramidal cell is higher than that required by meshing with four identical tetrahedrons.

In essence, Table I makes it clear that to obtain good results for simply shaped cavities we must use at least third-order bases when using very few cells. Furthermore, in our case, the mesh composed of 4 identical tetrahedra does not destroy the symmetry of the modes and is therefore able to use the DoFs in an optimal way, provided that bases of order higher than the fifth are used. In principle we can expect to obtain results as good as those shown in Table I (for $p = 6$) by using many more cells than done here, and bases of order lower than the third. Unfortunately, this turns out to be completely inconvenient because tens or hundreds of thousands of DoFs would be needed precisely because the number of DoFs that guarantees good results does not depend linearly on the order of the base used. On the other hand, we cannot think to improve the results simply by increasing the order of the bases used beyond the sixth because, as shown in Fig. 1, the condition number of the mass matrix (CN) grows exponentially with the order of the bases in use (regardless of the shape of the cells), and is already of the order of 10^6 for sixth-order bases. To improve the accuracy of the results of Table I (for $p = 6$) it becomes necessary to refine the mesh rather than further increase the order of the base used.

In any case, we are not interested in determining whether the best results in Table I for sixth-order bases are those obtained with the single pyramidal cell model rather than those obtained with four tetrahedral cells. What really matters is that we have never detected spurious modes using a single pyramidal cell. Since an analytical result is missing, we assume that for $p = 6$ the two meshes lead to results of equal accuracy; that is, the reference wavenumber (WN) in the central column of Table I is simply the average of the two values obtained using the two different meshes with $p = 6$. As shown in Fig. 2, the results obtained using a single cell and those obtained with four identical tetrahedral cells converge similarly to the reference WN as p and the number of DoFs increase.

The absence of spurious modes using a single cell needs to be verified considering structures meshed with multiple cells. Therefore, let us now consider the equilateral pyramid of Fig. 3, meshed with four pyramids of different aspect ratio which varies by varying the parameter s_v defined in the figure caption. The base of the yellow pyramid of Fig. 3 is always a square for $0 < s_v \leq 1/2$, therefore its Jacobian is constant at all points inside it. Conversely, the Jacobian inside the other three pyramids is polynomial (not constant), unless $s_v = 1/2$. Note that the yellow pyramid disappears for $s_v = 0$. This limiting case is not considered in the sequel because it relates to a mesh formed by one pyramid (the one in blue in Fig. 3) and two tetrahedrons (in white).

Fig. 4 reports, versus s_v, different results for the pyramidal cavity obtained with the meshes described in Fig. 3. The figure at top shows the percentage error on k for the first three modes,

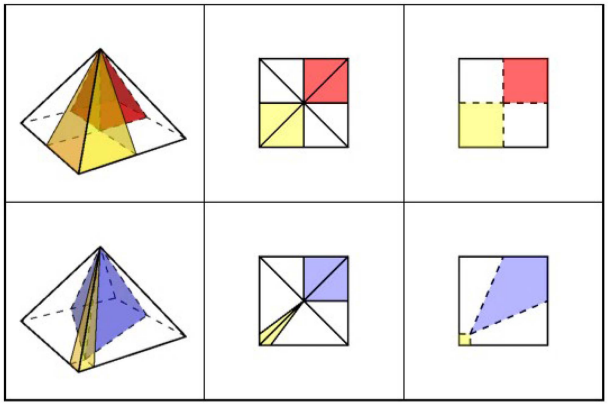

Fig. 3. On the left, an equilateral pyramid is meshed in various ways by four rectilinear pyramids of different aspect ratios that we define by assigning the position of their five vertices in the observer's space. The central column shows the pyramids seen from above, the right one the bases of the pyramids. In addition to the common apex, the four pyramids of the mesh also share a vertex located at the coordinate point $s = s_v$ along the diagonal going from southwest to northeast in the figures of the right column. The pyramid in yellow has a square base whatever the value of s_v, for s_v between 0 and 1/2. The meshes in the upper and lower row are obtained with $s_v = 1/2$ and $s_v = 1/8$, respectively. (The coordinate s_v is normalized w.r.t. the length of the diagonal of the base of the equilateral pyramid).

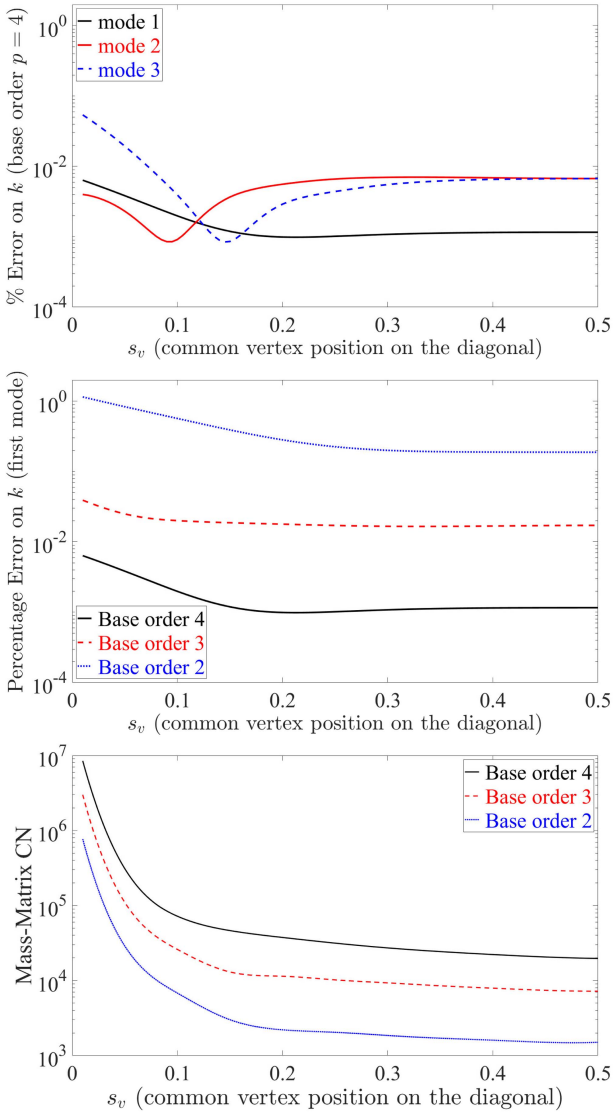

Fig. 4. Results obtained with the meshes in Fig. 3 by varying the s_v parameter.

obtained with the base of order $p = 4$. In the center the percentage error on k for the first mode only, obtained with bases of order 2, 3 and 4. Fig. 4 at bottom shows the condition number of the mass matrix as s_v varies, obtained with bases of order 2, 3 and 4.

The results of Fig. 4 show that the wavenumbers of the second and third modes coincide for $s_v = 0.5$ (symmetric mesh), and therefore have the same percentage error. This no longer happens if the mesh loses symmetry ($s_v < 0.5$) while, for sloppier meshes ($s_v < 0.1$) the errors increase, albeit slightly, and the CN increases (worsens) by a factor of the order of 10^3. These results prove the robustness of our pyramid bases.

III. Results for Rectangular Cavity Resonators

Let us consider a rectangular cross-sectional waveguide of length d closed by metal walls at both ends, that is the cavity resonator $\{x, y, z\colon 0 \le x \le a;\, 0 \le y \le b;\, 0 \le z \le d\}$. For this kind of cavities, the cartesian components of the eigenfields $\boldsymbol{e}$ and $\boldsymbol{h}$ are the product of three sinusoidal functions, one for each Cartesian variables x, y, z [15], [16]. For example, the longitudinal components e_z, h_z are

$$e_z = 0, \qquad h_z = \cos\left(\frac{m\pi x}{a}\right)\cos\left(\frac{n\pi y}{b}\right)\sin\left(\frac{p\pi z}{d}\right) \tag{3}$$

$$h_z = 0, \qquad e_z = \sin\left(\frac{m\pi x}{a}\right)\sin\left(\frac{n\pi y}{b}\right)\cos\left(\frac{p\pi z}{d}\right) \tag{4}$$

for the TE and the TM mode, respectively. Regardless of whether it is a TE or TM mode, the mode wavenumber

$$k = k_{mnp} = \sqrt{\left(\frac{m\pi}{a}\right)^2 + \left(\frac{n\pi}{b}\right)^2 + \left(\frac{p\pi}{d}\right)^2} \tag{5}$$

depends on the integer mode-numbers m, n, p, although there are no TE modes with mode index p equal to zero, nor TM modes with mode index m or n equal to zero, while there are both modes TE_{mnp} and TM_{mnp} with identical k if m, n and p are all non-zero.

Table II reports the wavenumbers k for two different cavities having dimensions a, b, d as in the Table. The results are obtained using the base of order $p = 4$ with a structured mesh made of only six pyramids, one for each face of the cavity, having a common apex at $(x, y, z) = (\frac{a}{2}, \frac{b}{2}, \frac{d}{2})$. This model produces 2,020 DoFs and 640 zero eigenvalues, with a mass matrix condition number of the order of 1.1×10^5 after diagonal preconditioning. The percentage error for the first 20 modes is shown in Fig. 5. The error is less than 0.1% for the first 18 modes and less than 0.5% for the first 37 modes. No spurious modes are observed. (We show the results for order $p = 4$ because this is a good compromise to obtain reduced computation times and achievable precision.)

Since each face of the cavity is the quadrilateral surface on which only one pyramid rests, the quality of the results depends on how well the basis functions approximate, inside each pyramid, the sinusoidal trend of the eigenfields in the three Cartesian

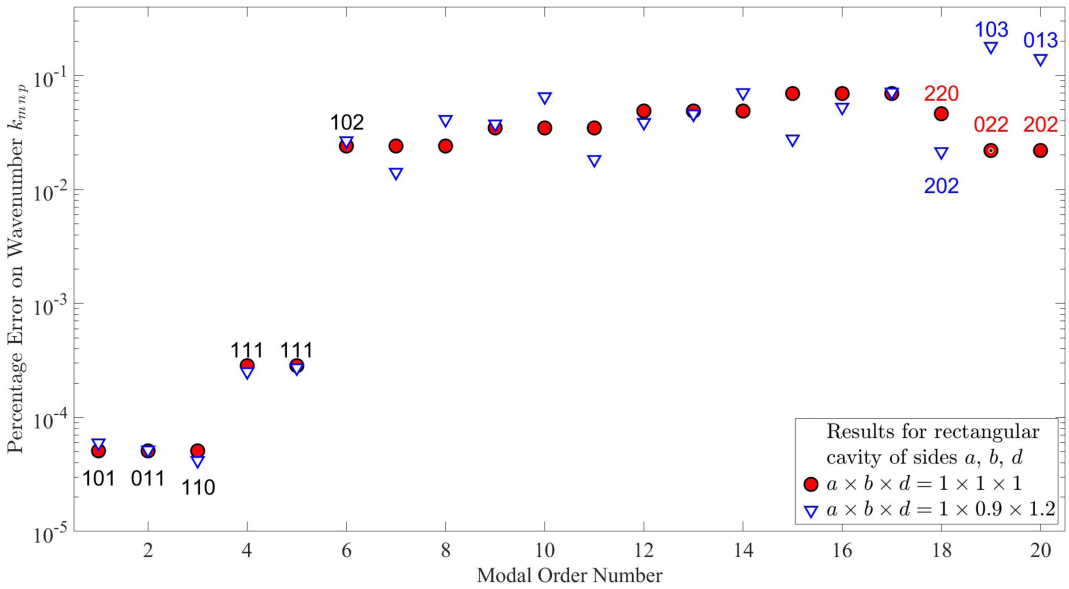

Fig. 5. Results for the rectangular cavities of Table II obtained with the pyramidal base of order four and a mesh of six pyramids. The figure reports the percentage error on the computed wavenumber with respect to the exact wavenumber (5), identified by the mode numbers m, n, p. These indices are reported only for some modes simply to clarify the trend of the error as their value increases.

TABLE II
RECTANGULAR CAVITY RESONATORS

Cavity of dimensions $a \times b \times d = 1 \times 0.9 \times 1.2$				
	$m\ n\ p$	k reference	k computed	% Error
1	101	4.089437	4.089440	6.0E-05
2	011	4.363323	4.363325	5.2E-05
3	110	4.696201	4.696203	4.2E-05
4	111	5.376634	5.376648	2.5E-04
5			5.376649	2.7E-04
6	102	6.106159	6.107802	2.7E-02
Cavity of dimensions $a \times b \times d = 1 \times 1 \times 1$				
	$m\ n\ p$	k reference	k computed	% Error
1	101	4.442883	4.442885	5.1E-05
2	011	4.442883	4.442885	5.1E-05
3	110	4.442883	4.442885	5.1E-05
4	111	5.441398	5.441414	2.8E-04
5				
6	102	7.024815	7.026504	2.4E-02

The Table shows the percentage error on k with respect to the reference value (5) identified by the mode numbers m,n,p for the first six modes of two different rectangular cavity resonators. Results obtained with 4th order base with a structured mesh made of only six pyramids.

directions, that is on the intervals $[0 \le x \le m\pi]$, $[0 \le y \le n\pi]$, and $[0 \le z \le p\pi]$. In fact, Fig. 5 clearly shows that every time the index m, n, or p increases by one unit, the accuracy of the results degrades.

To obtain results of quality close to that of Fig. 5 with zero-order basis functions and a structured mesh made up of pyramids we would need at least 10^7 unknowns which we may obtain by subdividing the cavity into N $\times$ N $\times$ N bricks, with $N \approx 100$ (see [12, §1.3]), and then define the usual 6 pyramids in each brick. (It goes without saying that if you are looking for quality results for the modes of an arbitrarily shaped cavity it is generally more convenient, in terms of CPU time, to immediately use brick or tetrahedral elements rather than pyramid cells everywhere.)

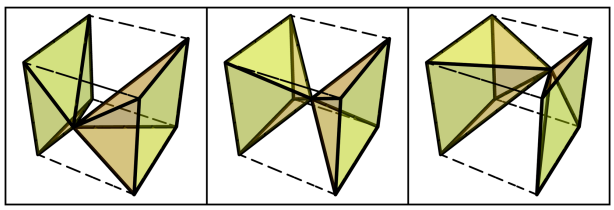

Fig. 6. A cube is meshed in different ways by six square-based rectilinear pyramids by varying the position of their common apex. In the figure the pyramids resting on the east and west faces of the cube are in yellow, the others are transparent. The common apex is located at the normalized coordinate point s on the diagonal joining the southwest vertex of the cube, where $s = 0$, to the northeast vertex, where $s = 1$. The six pyramids are identical if $s = 1/2$, as shown in the center. The left and right figures show the cases of $s = 1/4$ and $s = 3/4$, respectively.

The results that follow refer only to the cube-shaped cavity and are obtained with meshes of the type shown in Fig. 6, obtained by moving the apex in common to the 6 pyramids along the diagonal of the cavity of length $\sqrt{3}$. This model continues to have 2,020 DoF, but now the precision of the results is a function of the distance t between the apex and the corner, measured along the aforementioned diagonal by the normalized coordinate $s = t/\sqrt{3}$. Fig. 7 at top shows the error on k for the three fundamental modes of the cubic cavity (i.e., modes 101, 011, and 110), and for the next two modes (TE and TM 111). At bottom we show the mass-matrix condition number versus s.

So far we have shown results for the cube-shaped cavity obtained with a few cells in the mesh. As mentioned, we can increase the number of cells by replicating the "basic cube" several times, after having divided it into 6 pyramids, or into 5 tetrahedra as in Fig. 8. If we use sub-cubes divided into 5 tetrahedra, we must rotate each of them appropriately to guarantee mesh conformity. The average percentage error of the first 5 modes of the cubic cavity vs the number of DoFs is shown in Fig. 9 for varying base order. The straight-lines in Fig. 9 indicate the speed of convergence as the number of DoFs

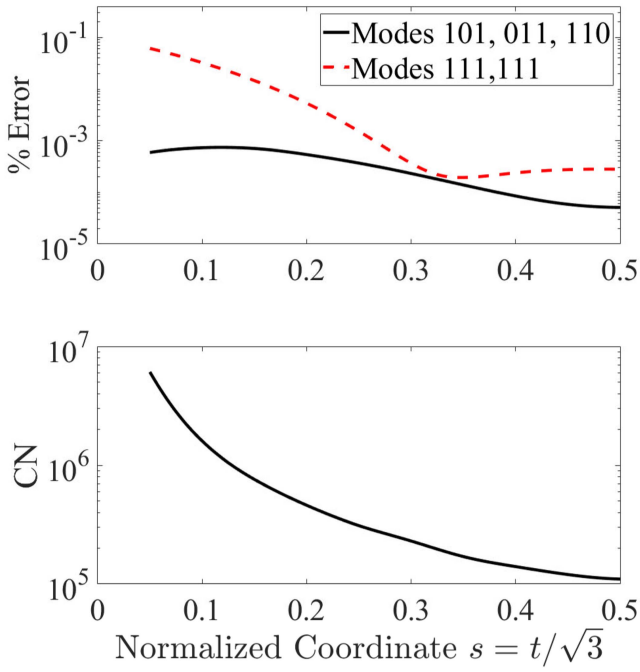

Fig. 7. Figure considers the cube cavity meshed with six pyramids having a common apex that varies along the diagonal of the cube of length $\sqrt{3}$, as described in Fig. 6. The results obtained with the fourth order base are shown with respect to the normalized apex-corner distance s. At top we show the percentage error on k for the first five modes; at bottom the CN mass matrix after diagonal preconditioning.

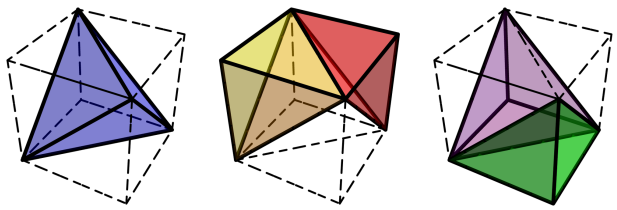

Fig. 8. A unit cube is divided into five tetrahedra by cutting off every other vertex; that is, four out of eight vertices, as shown in the figure on the left. On the left, the blue colored tetrahedron in the center of the cube is regular; that is, its edges have equal length. In the center and on the right we show the remaining tetrahedra two at a time, in different colors.

and the polynomial order of the elements used increase. Fig. 9 shows that the numerical solutions with tetrahedral or pyramidal mesh are more or less equivalent. However, we point out that, given the same order and (almost the same) number of DoFs, the CPU times required by a pyramidal mesh are higher than those required by a mesh entirely made up of tetrahedra.

Finally, for completeness, Fig. 10 shows the mass-matrix condition numbers relative to the cases in Fig. 9 versus the number of degrees of freedom. Note that in this case the CN obtained with the pyramidal meshes essentially depend only on the order of the base used because they relate to structured meshes formed by perfectly identical pyramids arranged in a perfectly symmetrical way, as shown in Fig. 6 in the center. Conversely, the CNs obtained with tetrahedral meshes increase as the number of degrees of freedom increases since these meshes are formed by tetrahedra of different aspect ratios, as shown in Fig. 8.

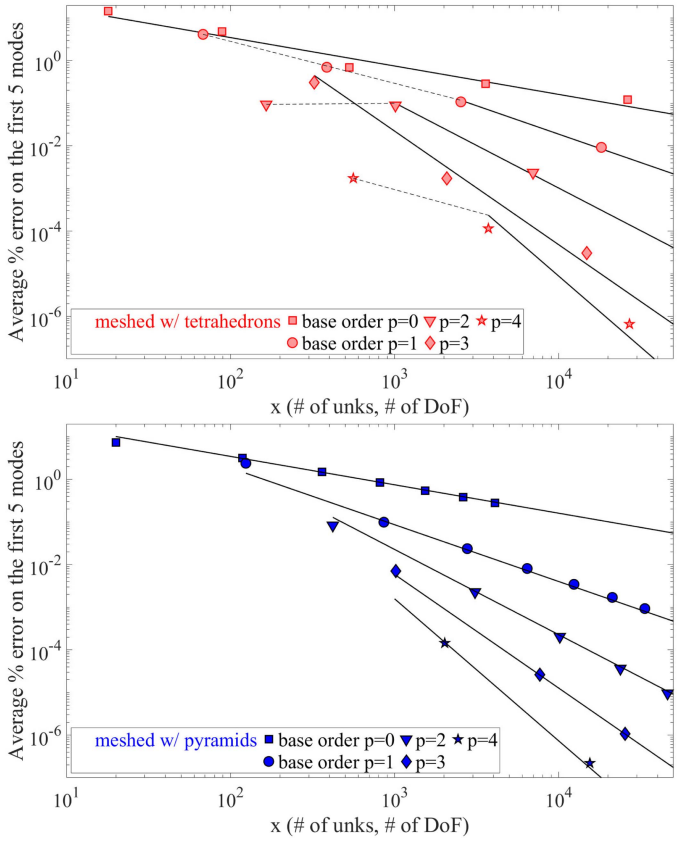

Fig. 9. Average percentage error for the first five modes of a cubic cavity obtained with elements of different order p. Meshes of different densities are obtained by first dividing the cavity into cubes, and then each cube into five tetrahedra (top figure) or six pyramids (bottom figure). The straight lines indicate the speed of convergence as the number of degrees of freedom and the polynomial order of the elements increase. The results at top were first presented in [17].

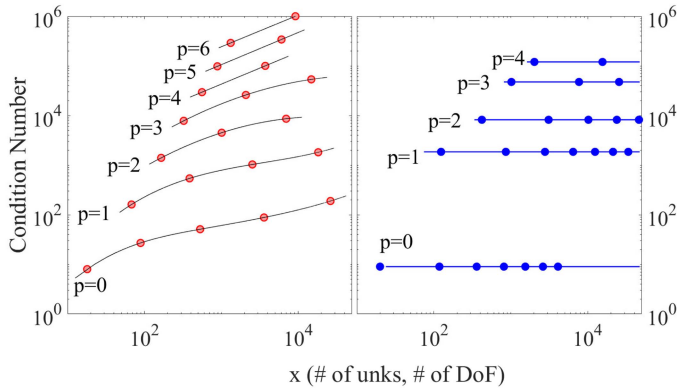

Fig. 10. Mass-matrix condition number related to the cases in Fig. 9. On the left the results obtained with tetrahedral cells, on the right those with pyramidal cells.

IV. Conclusion

This paper presents a whole set of test case results validating the new higher-order curl-conforming bases for pyramidal cells we have recently published. These basis functions are built to guarantee the continuity of the tangential components between adjacent elements of the same order but different shape, so that it is possible to build more efficient computer codes that

use hybrid meshes made with tetrahedra, bricks, prisms and quadrangular-based pyramids. The solutions of the various test cases discussed here are obtained using higher order elements or multipyramidal meshes or both, and the results are always compared with the solutions obtained with classical tetrahedral meshes using higher order bases. This allows us to verify that purely pyramidal meshes and elements give numerical results of comparable accuracy to those obtained with multitetrahedral meshes that use elements of the same order, essentially requiring the same number of degrees of freedom. The reported numerical examples show once again that higher order functions provide more accurate results than those obtainable with lower order elements. It is hoped that these results will facilitate the development of new electromagnetic solvers based on the use of hybrid meshes.

REFERENCES

[1] R. D. Graglia and P. Petrini, "Hierarchical curl-conforming vector bases for pyramid cells," *IEEE Trans. Antennas Propag.*, vol. 70, no. 7, pp. 5623–5635, Jul. 2022, doi: 10.1109/TAP.2022.3145430.

[2] R. D. Graglia, "Hierarchical divergence-conforming vector bases for pyramid cells," *IEEE Trans. Antennas Propag.*, early access, Feb. 6, 2023, doi: 10.1109/TAP.2023.3241443.

[3] F. Fuentes, B. Keith, L. Demkowicz, and S. Nagaraj, "Orientation embedded high order shape functions for the exact sequence elements of all shapes," *Comput. Math. Appl.*, vol. 70, pp. 353–458, 2015.

[4] F.-X. Zgainski, J.-L. Coulomb, Y. Maréchal, F. Claeyssen, and X. Brunotte, "A new family of finite elements: The pyramidal elements," *IEEE Trans. Magn.*, vol. 32, no. 3, pp. 1393–1396, May 1996.

[5] R. D. Graglia and I.-L. Gheorma, "Higher order interpolatory vector bases on pyramidal elements," *IEEE Trans. Antennas Propag.*, vol. 47, no. 5, pp. 775–782, May 1999.

[6] J.-L. Coulomb, F.-X. Zgainski, and Y. Maréchal, "A pyramidal element to link hexahedral, prismatic and tetrahedral edge finite elements," *IEEE Trans. Magn.*, vol. 33, no. 2, pp. 1362–1365, Mar. 1997.

[7] V. Gradinaru and R. Hiptmair, "Whitney elements on pyramids," *Electron. Trans. Numer. Anal.*, vol. 8, pp. 154–168, 1999.

[8] M. Bergot, G. Cohen, and M. Duruflé, "Higher-order finite elements for hybrid meshes using new nodal pyramidal elements," *J. Sci. Comput.*, vol. 42, no. 3, pp. 345–381, 2010. [Online]. Available: https://hal.archives-ouvertes.fr/hal-00454261

[9] N. Nigam and J. Phillips, "Numerical integration for high order pyramidal finite elements," *ESAIM, Math. Modelling Numer. Anal.*, vol. 46, no. 2, pp. 239–263, 2012, doi: 10.1051/m2an/2011042.

[10] M. Bergot and M. Duruflé, "High-order optimal edge elements for pyramids, prisms and hexahedra," *J. Comput. Phys.*, vol. 232, no. 1, pp. 189–213, Jan. 2013.

[11] A. Gillette, "Serendipity and tensor product affine pyramid finite elements," *SMAI J. Comput. Math.*, vol. 2, pp. 215–228, 2016, doi: 10.5802/smai-jcm.14.

[12] R. D. Graglia and A. F. Peterson, *Higher-Order Techniques in Computational Electromagnetics*. Edison, NJ, USA: SciTech Publishing/IET, 2016.

[13] J. Jaskowiec and N. Sukumar, "High-order symmetric cubature rules for tetrahedra and pyramids," *Int. J. Numer. Methods Eng.*, vol. 122, pp. 148–171, 2020, doi: 10.1002/nme.6528.

[14] R. D. Graglia and P. Petrini, "Pyramidal versus tetrahedral elements in finite element applications," in *Proc. Int. Conf. Electromagn. Adv. Appl.*, 2023, pp. 662–662, doi: 10.1109/ICEAA57318.2023.10297825.

[15] L. B. Felsen and N. Marcuvitz, *Radiation and Scattering of Waves*, Hoboken, NJ, USA: Wiley,1994.

[16] R. E. Collin, *Field Theory of Guided Waves*, 2nd ed. Hoboken, NJ, USA: Wiley, 1990.

[17] R. D. Graglia, P. Petrini, L. Matekovits, and A. F. Peterson, "Singular and hierarchical vector functions for multiscale problems," in *Proc. IEEE IEEE Int. Symp. Antennas Propag.*, 2016, pp. 239–240, doi: 10.1109/APS.2016.7695828.

Roberto D. Graglia (Life Fellow, IEEE) received the Laurea degree (*summa cum laude*) in electronic engineering from the Politecnico di Torino, Turin, Italy, in 1979, and the Ph.D. degree in electrical engineering and computer science from the University of Illinois at Chicago, Chicago, IL, USA, in 1983. From 1980 to 1981, he was a Research Engineer with the Centro Studi e Laboratori Telecomunicazioni, Turin. From 1981 to 1983, he was a Teaching and Research Assistant with the University of Illinois at Chicago, and later a Lecturer with the Politecnico di Torino from 1984 to 1991. From 1985 to 1992, he was a Researcher with the Italian National Research Council, where he supervised international research projects. In 1991 and 1993, he was an Associate Visiting Professor with the University of Illinois at Chicago. In 1992, he joined the Department of Electronics and Telecommunications, Politecnico di Torino, as an Associate Professor, where he has been a Professor of electrical engineering since 1999. He has authored or coauthored over 150 journal articles, book chapters, and conference proceedings. He is the coauthor of the book Higher-Order Techniques in Computational Electromagnetics (SciTech Publishing/IET, Edison, NJ, USA, 2016). His research interests include the numerical methods for high- and low-frequency electromagnetics, theoretical and computational aspects of scattering and interactions with complex media, waveguides, antennas, electromagnetic compatibility, and low-frequency phenomena. He has organized and offered several short courses in these areas for more than 25 years. Dr. Graglia was a Member of the IEEE Antennas and Propagation Society ADCOM from 2006 to 2008 and from 2014 to 2019, and the Chairperson of the IEEE Antennas and Propagation Society Meetings Committee from 2017 to 2020. In 2015, he was the President of the IEEE Antennas and Propagation Society. Since 1999, he has been the General Chairperson of the International Conference on Electromagnetics in Advanced Applications (ICEAA), and since 2011, he has been the General Chairperson of the IEEE-AP-S Topical Conference on Antennas and Propagation in Wireless Communications (IEEE-APWC). He was the recipient of the 2021 Harrington–Mittra Computational Electromagnetics Award. He was one of the three Guest Editors of the highly successful Special Issue of March 1997 on Advanced Numerical Techniques in Electromagnetics for the IEEE TRANSACTIONS ON ANTENNAS AND PROPAGATION, this Special Issue has received more than 3750 citations in the scientific literature up to December 2021. He was an Associate Editor for the IEEE TRANSACTIONS ON ANTENNAS AND PROPAGATION from 1995 to 1998, IEEE TRANSACTIONS ON ELECTROMAGNETIC COMPATIBILITY from 1998 to 2000, and IEEE ANTENNAS AND WIRELESS PROPAGATION LETTERS from 2002 to 2013, and he has been a Member of the Editorial Board of Electromagnetics since 1997. He was the International Union of Radio Science (URSI) for the Triennial International Symposia on Electromagnetic Theory as an Organizer of the Special Session on Electromagnetic Compatibility in 1998 and a co-organizer of the Special Session on Numerical Methods in 2004, and he was an Invited Convener at URSI General Assemblies for Special Sessions on Field and Waves in 1996, Electromagnetic Metrology in 1999, and Computational Electromagnetics in 1999. From 2009 to 2012, he was a Distinguished Lecturer of the IEEE Antennas and Propagation Society.

Paolo Petrini (Member, IEEE) was born in Torino, Italy, on October 4, 1955. He received the Laurea degree (*summa cum laude*) in electronic engineering from the Polytechnic of Turin, Turin, Italy, in 1979, with a graduation thesis on Integrated Optics, and the Ph.D. degree in electrical engineering from the Polytechnic of Turin, in 2018. In years 1980–1981, he was Research Engineer with CSELT, Italy, studying and measuring microwave subsystems for high speed PSK radio links, while in years 1981–1982, was Research Engineer with CERN (European Center for Nuclear Research, Geneva, Switzerland) involved in studying and measuring high Q cavities for beam acceleration. From 1983 to 2012, he was a Registered Engineer working in the fields of RF-Microwave and Aerospace engineering, with customers amongst the most important Companies in Europe. From 2012 to 2020, he was a Research Assistant with the Department of Electronics and Telecommunications of the Polytechnic of Turin. Since 2014, he has also been with the Department of Mechanical and Aerospace Engineering Telecommunications of the Polytechnic of Turin.

Open Access funding provided by 'Politecnico di Torino' within the CRUI CARE Agreement